

## IMAGING OF SDSS $z > 6$ QUASAR FIELDS: GRAVITATIONAL LENSING, COMPANION GALAXIES, AND THE HOST DARK MATTER HALOS<sup>1</sup>

CHRIS J. WILLOTT,<sup>2</sup> WILL J. PERCIVAL,<sup>3</sup> ROSS J. MCLURE,<sup>3</sup> DAVID CRAMPTON,<sup>2</sup> JOHN B. HUTCHINGS,<sup>2</sup>  
MATT J. JARVIS,<sup>4</sup> MARCIN SAWICKI,<sup>2</sup> AND LUC SIMARD<sup>2</sup>

*Received 2004 December 21; accepted 2005 March 7*

### ABSTRACT

We have undertaken deep optical imaging observations of three  $6.2 < z < 6.5$  quasar fields in the  $i'$  and  $z'$  filters. These data are used to search for foreground galaxies that are gravitationally lensing the quasars and distant galaxies physically associated with the quasars. Foreground galaxies are found closer than  $5''$  to the lines of sight of two of the three quasars. However, the faintness of these galaxies suggests that they have fairly low masses and provide only weak magnifications ( $\mu \lesssim 1.1$ ). No convincing galaxies physically associated with the quasars are found, and the number of  $i'$ -band dropouts is consistent with that found in random fields. We consider the expected dark matter halo masses that host these quasars under the assumption that a correlation between black hole mass and dark matter halo mass exists. We show that the steepness of the high-mass tail of the halo mass function at this redshift, combined with realistic amounts of scatter in this correlation, leads to expected halo masses substantially lower than previously believed. This analysis can explain the lack of companion galaxies found here and the low dynamical mass recently published for one of the quasars.

*Subject headings:* cosmology: observations — gravitational lensing — quasars: general

*Online material:* color figures

### 1. INTRODUCTION

Active supermassive black holes provide a useful means of locating very distant, massive galaxies. Studies of the host galaxies of luminous active galactic nuclei (AGNs) at redshifts up to  $z \approx 2$  show that they are associated with galaxies with luminous rest-frame optical stellar populations, corresponding to  $\gtrsim L_*$  (Kukula et al. 2001; Ridgway et al. 2001; Hutchings et al. 2002; Willott et al. 2003b; Dunlop et al. 2003). Furthermore, the strong correlation between black hole mass and stellar bulge luminosity and mass observed locally (Magorrian et al. 1998; Gebhardt et al. 2000; Ferrarese & Merritt 2000) shows that the most massive galaxies are those whose black holes have accreted the greatest mass and therefore were the most luminous AGNs.

It is now possible to discover luminous quasars out to a redshift of  $z = 6.4$ . Sources at this redshift are observed as they were  $\approx 13$  Gyr ago (93% of the age of the universe). The Sloan Digital Sky Survey (SDSS) has made a spectacular breakthrough in locating such quasars, and now 12 are known at  $z > 5.7$  (Fan et al. 2004). Black hole masses in these quasars are usually estimated by making the assumption that the quasars are accreting at the Eddington limit (e.g., Fan et al. 2001). This method is consistent with a black hole mass measurement from the kinematics of the broad emission-line gas (Willott et al. 2003a).

Under the Eddington argument, the black hole masses of these quasars are mostly in the range  $1\text{--}5 \times 10^9 M_\odot$ . These black hole masses could be much lower in the case of strong gravitational lensing or beaming. Observations so far have not shown such effects (Fan et al. 2003; Richards et al. 2004; Willott et al. 2003a).

The space density of these luminous SDSS quasars is extremely low,  $\rho = (6.4 \pm 2.4) \times 10^{-10} \text{ Mpc}^{-3}$  (Fan et al. 2004). The rarity of these objects and their large black hole masses makes it tempting to associate these quasars with the rarest peaks in the dark matter density distribution (Fan et al. 2001). The dark matter halos hosting the quasars would, under this hypothesis, have a mass of  $> 10^{13} M_\odot$ . Such halos would merge with smaller halos and in the present day would be identified as massive galaxy clusters, with a giant elliptical galaxy hosting the dormant supermassive black hole at the bottom of the potential well. However, it is also possible that the SDSS quasars reside in much more common, lower mass halos and that the correlation between halo mass and black hole mass is not well established at this early epoch. Determining the masses of the quasar host halos is extremely important for understanding the connection between black hole and galaxy growth in the early universe.

The evidence from submillimeter observations paints a rather confusing picture. On the one hand, thermal emission from dust has been detected from several of the quasars. These detections imply huge dust masses and star formation rates of several thousand  $M_\odot \text{ yr}^{-1}$  (Bertoldi et al. 2003a; Priddey et al. 2003). At this rate, the stellar mass of an  $L_*$  elliptical galaxy could be built up in  $\sim 0.1$  Gyr. The clustering of galaxies with such high star formation rates at lower redshift ( $z \sim 3$ ) is not well constrained, but early results suggest that these galaxies are associated with massive dark matter halos (Blain et al. 2004; although see Adelberger 2005). One of these quasars, SDSS J1148+5251, has also been detected in molecular carbon monoxide transitions (Bertoldi et al. 2003b; Walter et al. 2003). The CO spectra have a relatively narrow velocity profile with width  $280 \text{ km s}^{-1}$ . Walter et al. (2004) obtained high-resolution imaging of the CO

<sup>1</sup> Based on observations obtained at the Gemini Observatory, which is operated by the Association of Universities for Research in Astronomy, Inc., under a cooperative agreement with the National Science Foundation (NSF) on behalf of the Gemini partnership: the NSF (United States), the Particle Physics and Astronomy Research Council (United Kingdom), the National Research Council (Canada), CONICYT (Chile), the Australian Research Council (Australia), CNPq (Brazil), and CONICET (Argentina).

<sup>2</sup> Herzberg Institute of Astrophysics, National Research Council, 5071 West Saanich Road, Victoria, BC V9E 2E7, Canada; chris.willott@nrc.ca, david.crampton@nrc.ca, john.hutchings@nrc.ca, marcin.sawicki@nrc.ca, luc.simard@nrc.ca.

<sup>3</sup> Institute for Astronomy, University of Edinburgh, Royal Observatory, Blackford Hill, Edinburgh, EH9 3HJ, UK; wjp@roe.ac.uk, rjm@roe.ac.uk.

<sup>4</sup> Astrophysics, Department of Physics, University of Oxford, Keble Road, Oxford, OX1 3RH, UK; mjj@astro.ox.ac.uk.

TABLE 1  
GMOS-N IMAGING OBSERVATIONS

Quasar	Band	Exposure Time (s)	3 $\sigma$ Limiting Magnitude (AB)	Seeing (arcsec)
SDSS J1030+0524.....	$z'$	8100	26.3	0.68
SDSS J1048+4637.....	$z'$	5850	26.2	0.61
SDSS J1148+5251.....	$z'$	7650	26.2	0.65
SDSS J1030+0524.....	$i'$	9900	27.5	0.65
SDSS J1048+4637.....	$i'$	12150	27.7	0.54
SDSS J1148+5251.....	$i'$	13050	27.6	0.67

emission and confirmed that it comes from a compact structure (a few kiloparsecs). These observations allow a dynamical mass estimate for the mass within the central 2.5 kpc of the galaxy. This mass is comparable to the inferred molecular gas mass and is an order of magnitude lower than the mass predicted by assuming that this quasar resides in one of the rare peaks corresponding to dark matter halos of  $>10^{13} M_{\odot}$ . Although there are some uncertainties in the dynamical mass estimate, particularly in the geometry and inclination of the gas, this result casts serious doubt on the belief that the SDSS quasars pinpoint the most massive galaxies at high redshift.

Another approach to determining the mass of the quasar host dark matter halo is via a search for companion galaxies. If the SDSS quasars are formed in the rarest density peaks, then these correspond to large-scale overdense regions and hence the number of dark matter halos located nearby is substantially above the cosmic mean (Kaiser 1984; Barkana & Loeb 2004). Hence, the rarest peaks at  $z \approx 6$  are likely to be the sites of the first protoclusters. If the quasars really do occupy very massive halos, we would expect to see star-forming galaxies in their vicinity. To attempt to find these companion galaxies, we have carried out deep optical imaging around the three highest redshift quasars from the sample of Fan et al. (2003). In this paper we present these data and describe a search for foreground galaxies that may be gravitationally lensing the quasars and a search for star-forming galaxies at the quasar redshift. Finally, we discuss the implications for the host halos of the most distant quasars. Cosmological parameters of  $H_0 = 70 \text{ km s}^{-1} \text{ Mpc}^{-1}$ ,  $\Omega_M = 0.3$ , and  $\Omega_{\Lambda} = 0.7$  are assumed throughout.

## 2. OBSERVATIONS

We present observations for three quasars: SDSS J103027.10+052455.0 (SDSS J1030+0524;  $z = 6.30$ ), SDSS J104845.05+463718.3 (SDSS J1048+4637;  $z = 6.20$ ), and SDSS J114816.64+525150.3 (SDSS J1148+5251;  $z = 6.42$ ). The three quasar fields were imaged using the GMOS-N (Gemini Multi-Object Spectrograph North) imaging spectrograph on the Gemini North Telescope. GMOS-N uses an array of three 2048 pixel  $\times$  4608 pixel EEV CCD detectors. The pixel scale is  $0''.073 \text{ pixel}^{-1}$ , giving a useful field of view for imaging of  $5'.5 \times 5'.5$ . Since the typical seeing size of the observations is in the range  $0''.5 - 0''.7$ , the pixels were binned by a factor of 2 in both directions to speed up readout and data processing. The observations were carried out in queue mode during 2003 November and December. Typical exposure times are  $\approx 2$  hr in the  $z'$  band and  $\approx 3$  hr in the  $i'$  band. The relative exposure times were designed to give similar sensitivity in the two bands for very red objects with colors of  $i' - z' \approx 1.5$ . More details of the observations are given in Table 1.

The GMOS-N detectors have significant fringing at the red end of the optical wavelength regime. This is of particular

concern for the observations presented here that use the red  $i'$  and  $z'$  filters. The fringe pattern remains constant over time, so the fringes can be successfully removed if one obtains sufficient data to construct a high-signal-to-noise ratio fringe frame free of stars and galaxies. To enable the construction of these fringe frames, the observations of each field in each filter were split into 20–30 individual frames and the telescope was dithered in a  $3 \times 3$  pattern with offsets of  $10''$  in each direction. Median-combining all the data in each filter from the three fields enabled the construction of fringe frames free of astronomical objects.

Reduction of the imaging data was carried out using standard procedures. Most of the reductions were performed using tasks in the IRAF Gemini package that were specifically designed for GMOS. The first step is removal of the bias level using a bias frame constructed from many ( $>10$ ) bias observations (with the same binning) carried out during the same month. The images were flat fielded using flat-field frames generated from observations of the twilight sky. The three separate CCD images were then mosaicked together into one large image. The fringe frames generated from all observations within each filter were then scaled and subtracted from each image. All images were then inspected, and in some cases a different scaling was applied to better subtract the fringes. The images were then scaled to correct for atmospheric extinction.

All the images in each filter of the same field were then positionally registered using detected objects and were combined into one image rejecting pixels deviating by more than  $2.5 \sigma$  from the median and using a bad pixel mask. This method successfully removed CCD defects and cosmic rays while not rejecting counts from actual objects. The combined images still showed a low-level, large-scale, residual background, which varied across the images. The large-scale background was successfully removed by applying the background subtraction method of the SExtractor software (Bertin & Arnouts 1996) with a mesh size of  $19''$ . The  $i'$  images for each field were then shifted so that objects would appear in the same locations in the  $i'$  and  $z'$  images. Astrometry was performed by using the known geometric distortion of GMOS-N on the sky and setting the positions of the quasar targets to the positions given in the SDSS survey. Photometric calibration was achieved using photometric standard stars observed during the same nights as some of our observations.

## 3. OBJECT DETECTION, PHOTOMETRY, AND COMPLETENESS

Detection of objects in the images was performed using the SExtractor software. The  $z'$  band was selected as the primary detection waveband since  $z > 6$  galaxies are expected to have  $i' - z' > 2$  and may therefore be undetected at the  $i'$  band. SExtractor was run in double-image mode to determine  $i'$ -band measurements for objects detected in the  $z'$  band. The edges of

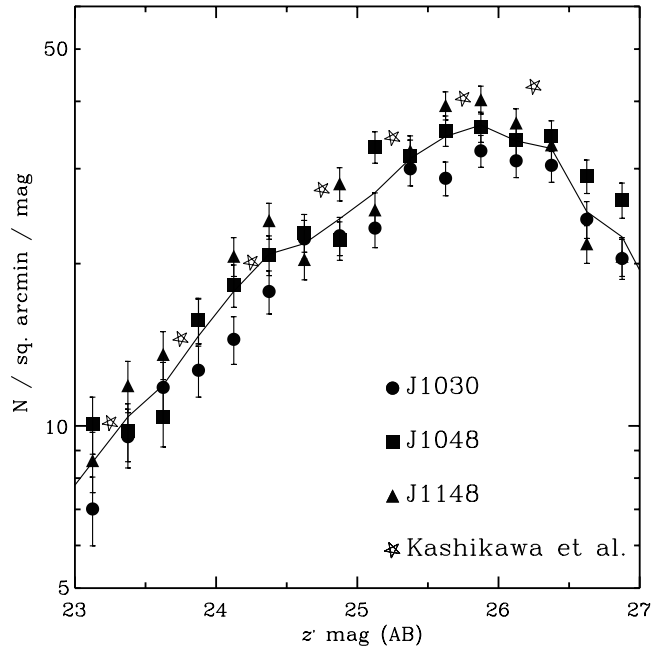


FIG. 1.—Binned number counts in the  $z'$  band in the fields of the three  $z > 6$  quasars. The  $z'$ -band magnitudes have been aperture-corrected using the prescription given in § 3. Error bars include only Poisson errors. The solid curve represents the mean counts averaged over the three fields. The stars show the  $z'$ -band number counts from the deeper and wider area Subaru Deep Field (Kashikawa et al. 2004). The counts are consistent, given the size of the error bars up to  $z' = 26$ . Beyond  $z' = 26$ , the quasar field counts turn over, indicating severe incompleteness. [See the electronic edition of the Journal for a color version of this figure.]

the images do not contain data at all dither positions and hence have lower sensitivity, contain artifacts, and have a varying background. Objects in these regions were excluded from the object catalogs. The useful area of the catalogs is 27, 27, and 28 arcmin<sup>2</sup> for SDSS J1030+0524, SDSS J1048+4637, and SDSS J1148+525, respectively.

Magnitudes on the AB system were measured in circular apertures of diameter  $1''.5$ . This size was chosen because it is greater than twice the seeing size, is much greater than the size scales of known  $z > 6$  galaxies (Bouwens et al. 2004), and has lower magnitude errors than larger apertures. Aperture corrections were applied statistically to the  $z'$ -band magnitudes by fitting a linear function to the difference between the total magnitude and aperture magnitude as a function of aperture magnitude. The best-fit relation is  $z'_{\text{tot}} - z'_{\text{ap}} = 3.58 - 0.133z'_{\text{ap}}$ , which gives an aperture correction of 0.25 mag at  $z' = 25$ . Note that this relation leads to large aperture corrections at bright magnitudes, which may be inappropriate for compact sources such as stars, but we are in general only interested in faint objects, for which the aperture corrections are reasonable ( $z' > 23$ ). A similar procedure was not adopted for the  $i'$ -band magnitudes, since the uncorrected aperture magnitudes are used to measure the  $i' - z'$  colors.

The rms noise in the sky background was measured to determine the magnitude limits of the images. Magnitude limits are quoted as  $3\sigma$  limits in  $1''.5$  apertures. Typical magnitude limits are  $z' \approx 26.2$  and  $i' \approx 27.6$  (see Table 1). The relative depths of the images are suitable for detecting very red objects with  $i' - z' > 1.5$ .

To assess the completeness of the  $z'$ -band catalogs, we consider both the observed number counts and the recovery of simulated objects. Binned number counts for the  $z'$ -band im-

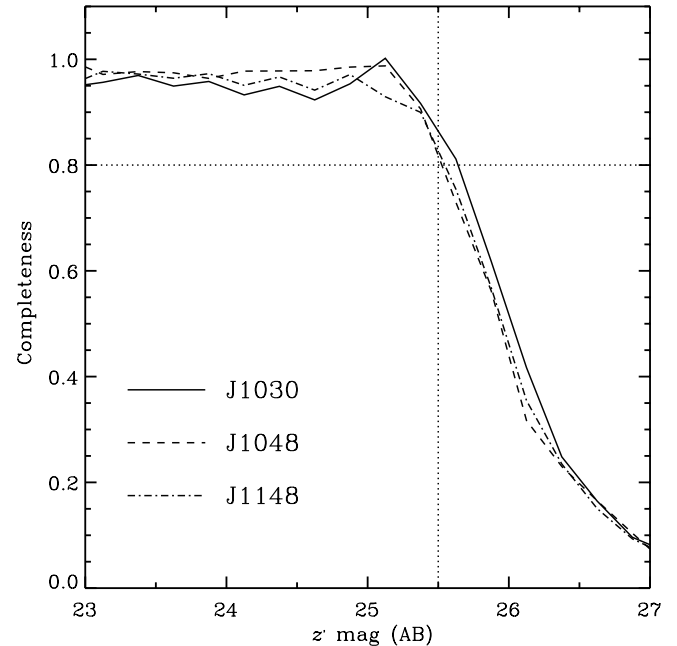


FIG. 2.—Completeness ratio vs. aperture-corrected  $z'$ -band magnitudes derived from recovery of simulated galaxies, as detailed in § 3. The curves are quite similar for the three different fields. Dotted lines indicate the location of a completeness ratio of 0.8 and the adopted complete magnitude limit of  $z' = 25.5$ . [See the electronic edition of the Journal for a color version of this figure.]

ages for all three fields are shown in Figure 1. The counts in the three fields do not differ significantly from each other. They agree well with the  $z'$ -band counts determined from a deeper and much larger area survey (0.2 deg<sup>2</sup>, or 30 times the GMOS-N field of view) of the Subaru Deep Field (SDF) by Kashikawa et al. (2004). The number counts in the quasar fields begin to change slope at  $z' > 25.5$  and turn over at  $z' = 26$ , indicating that this is where the sample becomes incomplete.

The source recovery as a function of magnitude was determined by populating the images with artificial galaxies and then using SExtractor to attempt to detect these objects. About 10,000 artificial galaxies with magnitudes in the range  $23 < z' < 27$  were placed into copies of the  $z'$  images of each quasar. Regions of the images already occupied by objects were masked out of the process to eliminate incompleteness due to blending. SExtractor was run twice: first on images containing only the artificial galaxies and a very low noise level and then on the actual quasar field images with the artificial galaxies inserted. The ratio of the number of artificial objects detected in the quasar field images to the number in the low-noise images gives the completeness. This completeness ratio is plotted as a function of magnitude for the three quasar fields in Figure 2. The completeness in all the fields is fairly flat at close to 1 up to  $z' = 25.2$  and then begins to decline. The rapid decline occurs at  $z' > 25.5$ , and the completeness drops to 0.5 by  $z' = 26.0$ . All the fields have completeness  $> 0.8$  at  $z' = 25.5$ , and we adopt this as the magnitude at which completeness begins to become an issue. This analysis with simulated objects agrees well with the results for the number counts discussed previously.

#### 4. SEARCH FOR FOREGROUND GALAXIES LENSING THE QUASARS

The combined effects of a steep luminosity function and the high optical depth to  $z \sim 6$  mean that gravitational lensing is expected to be particularly important for surveys of luminous

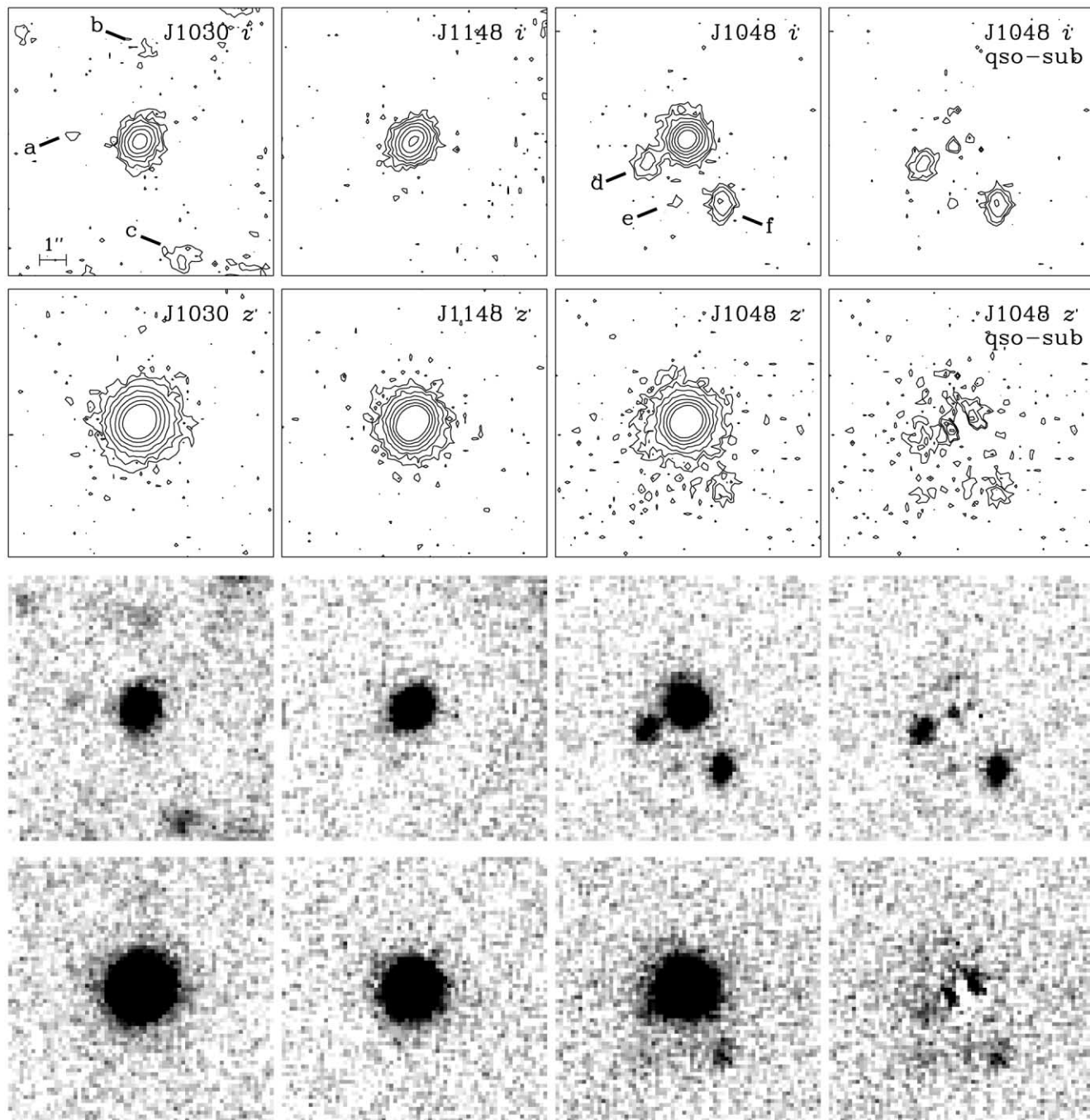


FIG. 3.—GMOS images in the  $i'$  and  $z'$  bands, centered on the three quasars SDSS J1030+0524, SDSS J1148+5251, and SDSS J1048+4637 (left to right). The rightmost column shows the images of SDSS J1048+4637 after subtracting off a scaled point-spread function (PSF) at the location of the quasar to show more clearly the nearby galaxies. There are some residuals from the PSF subtraction process that tests on stars in the field show are likely to be artifacts. Each box is  $10''$  on a side, centered on the quasar, with north up and east to the left. Contour plots are shown with a logarithmic scale at approximately 1.5, 3, 5, 9, 17, 31, and 56 times the background rms per pixel. Gray-scale plots have a linear stretch ranging from  $-0.5$  times the background rms (white) to  $+4$  times the background rms (black).

quasars at high redshift, such as the SDSS  $z > 5.7$  quasar survey. Predictions for the fraction of multiply imaged quasars in the SDSS for various forms of the luminosity function have been made by Wyithe & Loeb (2002a, 2002b) and Comerford et al. (2002). Fan et al. (2003) and Richards et al. (2004) discuss high-resolution imaging (ranging from  $0''.1$  to  $0''.8$ ) of all seven  $z > 5.7$  quasars known at the time and found that none of them appear to be multiply imaged. However, the lack of multiple images of the SDSS quasars does not necessarily mean that lensing is unimportant. For simple singular isothermal sphere

models the magnification is  $\mu < 2$  if the source is singly imaged. More realistic potentials, including isothermal ellipsoids, cluster-scale halos, and microlensing, can give rise to higher magnifications for singly imaged quasars (Keeton et al. 2005; Wyithe & Loeb 2002b).

Shioya et al. (2002) found a faint galaxy close to the line of sight of the  $z = 5.74$  quasar SDSS J1044–0125. The lensing galaxy has a magnitude of  $i'(AB) = 24.3$ , a separation from the quasar of  $\theta = 1''.9$ , and a likely redshift in the range  $1.5 < z < 2.5$ . Spurred on by this discovery, this group observed two

TABLE 2  
OBJECTS DETECTED WITHIN  $5''$  OF THE QUASARS

OBJECT	OBJECT POSITION (J2000)		$\theta$ (arcsec)	$i'$ (AB)	$z'$ (AB)
	R.A.	Decl.			
a.....	10 30 27.26	+05 24 55.3	2.5	$27.54 \pm 0.35$	$>26.3$
b.....	10 30 27.08	+05 24 58.2	3.5	$26.69 \pm 0.17$	$26.12 \pm 0.28$
c.....	10 30 26.99	+05 24 50.6	4.6	$26.05 \pm 0.10$	$>26.3$
d.....	10 48 45.19	+46 37 17.4	1.7	$25.67 \pm 0.05$	$24.97 \pm 0.11$
e.....	10 48 45.10	+46 37 16.1	2.2	$27.32 \pm 0.22$	$>26.2$
f.....	10 48 44.92	+46 37 15.9	2.7	$25.37 \pm 0.04$	$24.82 \pm 0.10$

NOTES.—Objects detected at the  $i'$  band within a  $5''$  radius of the quasars. Three objects were detected in each of the fields of SDSS J1030+0524 and SDSS J1048+4637. Nothing was detected within  $5''$  of SDSS J1148+5251. “Object” refers to the labels in Fig. 3. Units of right ascension are hours, minutes, and seconds, and units of declination are degrees, arcminutes, and arcseconds. “ $\theta$ ” is the separation of the object and the quasar. Magnitudes are given as observed in a  $1.75$  diameter aperture. Limits at the  $z'$  band are  $3\sigma$  in the same size aperture.

more high-redshift quasar fields (SDSS J1030+0524 at  $z = 6.30$  and SDSS J1306+0356 at  $z = 5.99$ ) but failed to find galaxies projected closer than  $6''$  and  $3''$  to these quasars, respectively (Yamada et al. 2003).

We have imaged three quasar fields, and in this section we use our data to search for foreground galaxies that may be lensing the quasars. One of these fields, SDSS J1030+0524, has been imaged before by Yamada et al. (2003), but our images are 1–2 mag deeper and have better resolution than those in Yamada et al. and Shioya et al. (2002). Images of the regions surrounding the quasars are shown in Figure 3. Contours and gray scales are shown for the same fields to highlight different aspects of these high dynamic range images. The contours show smooth isophotes in the quasar flux, which rule out the existence of very close, bright companion galaxies and gravitational lensing image splitting in the quasars at the limit of our resolution. The ellipticities and FWHMs of the quasars are consistent with those of stars in the images.

We searched for objects close to the quasars by inspection of smoothed images. We only consider objects within a  $5''$  radius of the quasars, since lensing by galaxy-sized masses is only effective with impact parameters of a few arcseconds. In addition, the probability of finding a galaxy at random within a circle of  $5''$  radius is large at the magnitude limit of the  $i'$ -band images (this probability is 0.9 for  $i' < 27$ ).

Three galaxies were detected in the fields of each of SDSS J1030+0524 (labeled a, b, and c) and SDSS J1048+4637 (labeled d, e, and f), and none were detected in the field of SDSS J1148+5251. The details of these galaxies are given in Table 2. All of these galaxies are visible in the  $i'$  band, and their  $i' - z'$  colors (or color limits) show that they are foreground to the quasars. For SDSS J1030+0524, the objects are all rather faint ( $i' > 26$ ) and distant from the quasar ( $\geq 2.5''$ ). For SDSS J1048+4637, the closest galaxy (d) is only  $1.7''$  from the quasar. To measure accurate photometry for this galaxy it was necessary to subtract the bright unresolved quasar from the image (Fig. 3, right). Galaxy d has  $1.75$  aperture magnitudes of  $i' = 25.67 \pm 0.05$  and  $z' = 24.97 \pm 0.11$ . The galaxy  $2.7''$  from the quasar (galaxy f) has similar magnitudes. Both these galaxies have fairly red colors, with  $i' - z' = 0.70$  and  $0.55$ , respectively. Only 20% of galaxies in our images with similar magnitudes have  $i' - z' > 0.5$ .

#### 4.1. Lensing Galaxy Masses, Redshifts, and Magnifications

In order to determine the lensing magnification due to such galaxies, one needs to know the galaxy mass (or, equivalently,

the velocity dispersion) and the redshift. Under the simplifying assumption that the lens potential can be modeled as an isothermal sphere, the magnification  $\mu$  is  $\mu = \theta/(\theta - \theta_E)$ , where  $\theta$  is the angle from the lens galaxy to the source and  $\theta_E$  is the Einstein radius given by  $\theta_E = 4\pi(\sigma_v/c)^2(D_{LS}/D_{OS})$ , where  $D_{LS}$  is the lens-source angular diameter distance and  $D_{OS}$  is the observer-source angular diameter distance.

Neither the masses nor the redshifts are strongly constrained by our photometric observations, but we use the information available to determine likely values. The red color of  $i' - z' = 0.70$  for galaxy d close to SDSS J1048+4637 is not consistent with the color of known galaxies at low redshifts. Therefore, we can at least put a lower limit on the redshift of this galaxy. Also, galaxy colors at high redshifts are expected to be blue in the absence of dust reddening, due to the prominence of young stellar populations. We used the HyperZ code (Bolzonella et al. 2000) with the two photometric points to determine if this color leads to any constraints on the redshift. Using a range of evolving galaxy templates with moderate dust reddening ( $0 \leq A_V \leq 0.5$ ), we find that a 90% confidence range for the redshift is  $0.4 < z < 2.1$ . There is also a secondary solution at  $5.1 < z < 5.5$ , where the red color is due to the Lyman break entering the  $i'$  band. If we consider the redshift distribution of galaxies of this magnitude, it is most plausible that the galaxy is at the lower redshift range. Note that if this galaxy is *highly* reddened by dust, then the redshift is no longer well constrained.

The mass or stellar velocity dispersion of the galaxy can be estimated from the photometry by assuming a redshift and a star formation history. Given the red color of this galaxy, we assume that it is an early type that has undergone passive evolution after a starburst at high redshift and use the evolving elliptical galaxy template from Bruzual & Charlot (2003) that formed at  $z = 7$  (the exact formation redshift assumed does not critically change the results presented here). The correlation between  $i'$ -band absolute magnitude and  $\sigma_v$  observed at low redshifts (Bernardi et al. 2003) was used to relate the evolved absolute magnitude to  $\sigma_v$ . For three possible lens redshifts of  $z = 0.4, 1,$  and  $2$ , the calculated stellar velocity dispersions are  $\sigma_v = 55, 87,$  and  $127 \text{ km s}^{-1}$ , respectively. Note that the Bernardi et al. relation is only derived for  $z < 0.3$  and  $\sigma_v > 100 \text{ km s}^{-1}$ , so its use here involves extrapolation in both redshift and velocity dispersion. Given that the redshift of the source is  $z = 6.20$  and  $\theta = 1.7''$ , this leads to Einstein radii of  $\theta_E = 0.07, 0.13,$  and  $0.18''$  and magnifications of  $\mu = 1.04, 1.08,$  and  $1.12$  for lens redshifts of  $z = 0.4, 1,$  and  $2$ , respectively.

It is clear that, whatever the redshift of this lensing galaxy, it is not very massive and provides only a small magnification to

the flux of SDSS J1048+4637. Therefore, it makes a negligible difference to the derived luminosity and black hole mass. Given that the closest galaxy to SDSS J1030+0524 (galaxy a) is even fainter and farther away, the magnification in that case is even lower. An increase in the magnification could come about if (1) the galaxy lies in a moderately rich high-redshift cluster or (2) the galaxy resides in a dark matter halo with a higher than average mass-to-light ratio.

For SDSS J1044–0125, Shioya et al. (2002) estimated the lens galaxy to have a velocity dispersion of  $\sigma_v \sim 200 \text{ km s}^{-1}$  and to be located at redshift  $z \approx 2$ . According to Shioya et al., this would give a magnification of  $\mu = 2$ . However, we have repeated their calculations and find their values for the Einstein radius and magnification to be erroneous (this error is also present in Yamada et al. [2003]). For  $z = 2$  and  $\sigma_v = 200 \text{ km s}^{-1}$ , the magnification is actually  $\mu = 1.3$ . The range of plausible lens redshift and velocity dispersion combinations given in their paper lead to a range of  $1.1 < \mu < 1.5$ . As with SDSS J1048+4637, the corrections to the derived luminosity and black hole mass of SDSS J1044–0125 are small.

### 5. SEARCH FOR $z > 6$ GALAXIES IN THE QUASAR FIELDS

Galaxies at redshifts of  $z > 5.7$  can be identified by the sharp drop in flux across the Lyman break, leading to a very red  $i' - z'$  color. The  $z > 6$  SDSS quasars have  $z' \approx 20$  and colors measured from our images of  $i' - z' = 3.25$ , 2.98, and 3.25, respectively, for SDSS J1030+0524, SDSS J1048+4637, and SDSS J1148+5251. The spectra of quasars and star-forming galaxies over the rest-frame wavelength range 90–140 nm probed by the  $i'$  and  $z'$  filters are dominated by a large break due to absorption by neutral hydrogen. Therefore, one would expect companion galaxies to have comparable  $i' - z'$  colors to the quasars. The fact that the light from a companion galaxy would pass through intergalactic medium (IGM) neighboring that which the quasar light passes through further strengthens the idea that the colors of companion galaxies are expected to be  $i' - z' \approx 3$ .

Simulated color-magnitude tracks for two different types of galaxy as a function of redshift are shown in Figure 4. Model galaxy spectra were generated from the Bruzual & Charlot (2003) spectral synthesis code with Lyman forest absorption evolution matching the observations of Songaila & Cowie (2002). The upper curve represents a present-day  $L_*$  elliptical galaxy that formed all of its stars in a starburst starting at a redshift of  $z = 10$  with a characteristic timescale of 1 Gyr and has evolved since without merging. There is no dust extinction assumed for this model, but in reality the dust extinction would increase with redshift (due to evolution and  $k$ -correction), making the galaxy redder and fainter than is plotted at higher redshifts. The lower curve represents a  $L_*$  Lyman break galaxy model in which the galaxy is observed 0.5 Gyr into a constant star formation rate starburst. It is clear that the only possible low-redshift contaminants with  $i' - z' > 1.5$  are galaxies with a high level of dust reddening.

Also plotted in Figure 4 are color-magnitude diagrams constructed from the  $z'$ -band–selected catalogs described in § 3 for each of the three quasar fields. Most objects have colors in the range  $0 < i' - z' < 1$ , as is well known from previous surveys (Dickinson et al. 2004; Capak et al. 2004). These colors are in agreement with the model galaxy tracks at  $z < 5$ .

A search was made for objects that could plausibly be high-redshift galaxies. The  $i'$ -band dropout selection criteria adopted were a signal-to-noise ratio in the  $z'$  band of  $\geq 4$  and a color of

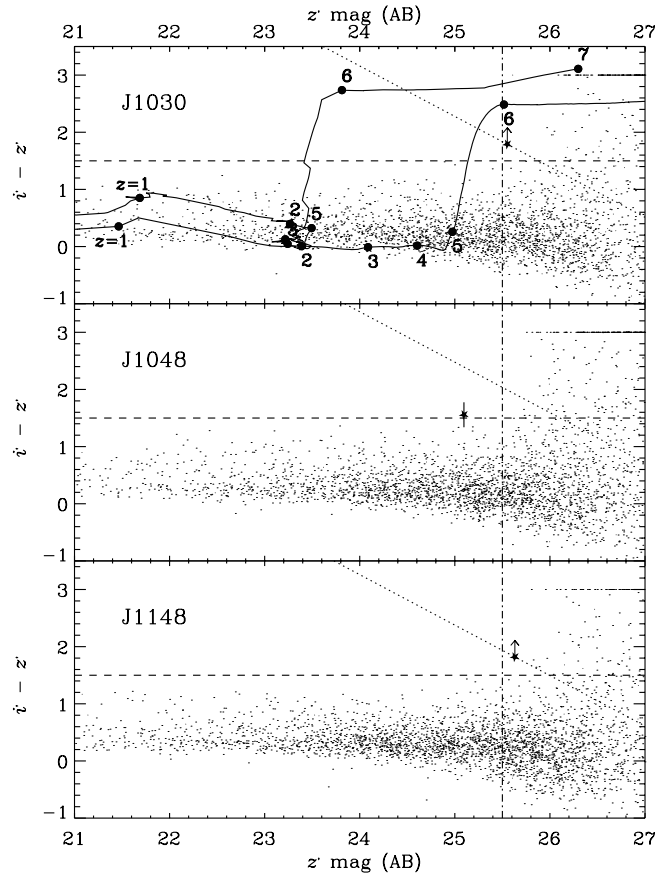


FIG. 4.—Color-magnitude (aperture-corrected) diagrams for objects detected in the  $z'$  band in the quasar fields. The completeness limit of  $z' = 25.5$  is shown with a dot-dashed line. The high-redshift galaxy selection criterion of  $i' - z' > 1.5$  is marked with dashed lines. The dotted lines represent the color of an object that is just detected at the  $3 \sigma$  level in the  $i'$  band as a function of the  $z'$ -band magnitude. Most objects with measured zero or negative flux in the  $i'$  band are plotted at  $i' - z' = 3$ . The exceptions to this are objects that pass the  $i'$ -band dropout selection criteria discussed in § 5. These are shown with star symbols and lower limits on the  $i'$ -band  $3 \sigma$  line. The dots at  $i' - z' > 1.5$  indicate sources that are detected at less than  $4 \sigma$  at the  $z'$  band and hence have very large uncertainties on their magnitudes and colors and in some cases may be spurious. The labeled curves show the color and magnitude as a function of redshift for an evolving  $L_*$  elliptical galaxy (upper curve) and a nonevolving  $L_*$  Lyman break galaxy (lower curve); see text for more details. [See the electronic edition of the Journal for a color version of this figure.]

$i' - z' \geq 1.5$ . Possible candidates were inspected, and magnitudes were checked to ensure that their unusual color were not spurious. A total of three objects satisfying these criteria were found; these are shown with filled symbols in Figure 4. These all have magnitudes in the range  $25 < z' < 26$ , and only one of them is detected at the  $3 \sigma$  level at the  $i'$  band. This object has  $z' = 25.10$  and a color of  $i' - z' = 1.56 \pm 0.22$ . The other two objects have  $z' \approx 25.6$  and only lower limits on their  $i' - z'$  color, which lie in the range 1.7–1.9.

In § 3 we showed that our  $z'$ -band images are complete to  $z' = 25.5$  at a level greater than 80%. Figure 4 shows that at  $z' \leq 25.5$ , every single  $z'$ -band object detected on our images has a counterpart at the  $>3 \sigma$  level in the  $i'$ -band image. At fainter magnitudes, this is no longer true, and our constraints on the  $i' - z'$  colors of objects at these magnitudes becomes very weak due to uncertainty in both the  $z'$  and  $i'$  magnitudes. Therefore, we limit further analysis to objects brighter than the magnitude limit of  $z' = 25.5$ .

At  $z' < 25.5$  we find one  $i'$ -band dropout in the three quasar fields. This object has  $i' - z' = 1.56 \pm 0.22$ , which is quite close to the color selection value, and the size of the uncertainty means that it is quite plausible that photometric errors have scattered the color into the dropout range. The measured color is about  $7\sigma$  away from the colors of the SDSS quasars, which suggests that if it is a high-redshift galaxy, then it is most likely foreground to the quasars with a redshift in the range  $5.7 < z < 6$ . The galaxy is located a projected distance of  $81''$  from the quasar (approximately halfway from the quasar to the edge of the GMOS field). Therefore, we conclude that there are no plausible galaxies brighter than  $z' = 25.5$  associated with any of these three quasars.

We now consider the number of  $i'$ -band dropouts we could have expected to find under the assumption that the quasar fields are random and show no enhancement due to the existence of the quasars. The best comparison data sets that go deep enough over a wide area are the *Hubble Space Telescope* Advanced Camera for Surveys (ACS) imaging of the Great Observatories Origins Deep Survey (GOODS) regions (Giavalisco et al. 2004) and the Subaru Deep Field (Kashikawa et al. 2004). These observations give a surface density of objects with  $z' < 25.5$  and  $i' - z' > 1.5$  of  $0.01\text{--}0.02$  arcmin $^{-2}$  (Dickinson et al. 2004; Bouwens et al. 2004; Nagao et al. 2004). The total sky area we have surveyed with GMOS-N is  $82$  arcmin $^2$ . Therefore, on the basis of the GOODS and SDF observations we would expect  $\approx 1\text{--}2$   $i'$ -band dropouts in our total area. Our finding of one dropout is entirely consistent with the expectations for a blank field.

The results presented in this section show that these quasar fields do not exhibit an excess of luminous companion galaxies. The magnitude limit of  $z' = 25.5$  corresponds to a UV luminosity of  $L_{1500} = 2.5 \times 10^{29}$  ergs s $^{-1}$  Hz $^{-1}$  at a redshift of  $z = 6.3$ . This is equivalent to  $2L_*$  in the  $z \approx 6$  galaxy luminosity function (Bunker et al. 2004) and an unobscured star formation rate of  $\text{SFR} = 30 M_{\odot} \text{ yr}^{-1}$ , assuming the conversion given in Madau et al. (1998). The few known galaxies at redshifts  $z \approx 6.6$  discovered in narrowband surveys have star formation rates derived from their UV luminosities that are comparable to this limit (Hu et al. 2002; Kodaira et al. 2003). For comparison, the millimeter detections of dust in SDSS J1048+4637 and SDSS J1148+5251 imply total star formation rates of  $>1000 M_{\odot} \text{ yr}^{-1}$  in the host galaxies of the quasars (Bertoldi et al. 2003a).

A study similar to ours has recently been reported by Stiavelli et al. (2005). They have observed the quasar SDSS J1030+0524 with ACS on the *Hubble Space Telescope* in the  $i_{775}$  and  $z_{850}$  filters. Their data reaches slightly deeper than ours, and they identify seven objects with  $i_{775} - z_{850} > 1.5$  in the quasar field. Only 3% of randomly selected areas in the GOODS fields show such a high density of red objects, indicating an excess in the field of this quasar. The single  $i' - z' > 1.5$  object we discovered in the field of SDSS J1030+0524, which is plotted on Figure 4, is also found by Stiavelli et al., and a high-resolution image of it is shown in their Figure 2 (*top*). Four of the seven objects found with ACS are detected at  $i_{775}$  and have  $i_{775} - z_{850} < 2$ . These objects are not red enough to be located at a redshift similar to the quasar (Dickinson et al. 2004). A spectroscopic redshift has been obtained for one object, and it reveals a redshift of  $z = 5.970$ . The large redshift difference between the quasar and this galaxy means that if they are part of the same large-scale overdensity, then the comoving scale of that structure is larger than anything found in the low-redshift universe (Pandey & Bharadwaj 2005).

## 6. CONSTRAINTS ON THE DARK MATTER HALO MASSES

Early-type galaxies in rich clusters in the local universe show homogeneous, old stellar populations, suggesting coeval star formation at high redshifts (e.g., López-Cruz et al. 2004). Therefore, if the quasars (two of which have far-IR luminosities indicating vigorous star formation) are in protocluster environments, one would expect to see massive companion galaxies forming stars. It has been suggested that there could be a suppression of star formation in the vicinity of a strong UV photoionizing field, such as that of a quasar (Couchman & Rees 1986). This is because the radiation would heat the diffuse gas in the IGM to a temperature of  $T \sim 1000$  K and inhibit the cooling process by which gas condenses to form stars. However, these effects are likely to be significant only in low-mass halos and are not such an issue for the more massive halos hosting galaxies with  $\text{SFR} > 30 M_{\odot} \text{ yr}^{-1}$  that we are sensitive to.

The goal of our observations was to constrain the masses of the dark matter halos hosting these quasars by considering the clustering of star-forming galaxies around them. In fact, we have been unable to identify any companion galaxies, suggesting that these quasars may not be residing in the most massive halos at this epoch, in line with the dynamical mass measurement of the host galaxy of SDSS J1148+5251 by Walter et al. (2004). However, given the large uncertainties in transforming from observable quantities such as UV star formation rate to typical Lyman break halo mass and duty cycle at  $z > 6$ , it is difficult to directly turn our nondetection into a robust upper limit for the halo masses. In this section we show that scatter in the  $M_{\text{BH}}\text{--}M_{\text{DM}}$  relation, combined with a steeply falling mass function, biases the host halo masses of the observed high-redshift quasars to lower values, suggesting that the inferred low host halo masses do not necessarily imply a breakdown of the low redshift  $M_{\text{BH}}\text{--}M_{\text{DM}}$  correlation at  $z > 6$ .

An upper limit on the halo mass hosting luminous quasars can be calculated from a comparison of their space densities. This method assumes that quasars reside in the most massive halos, which exist in sufficient quantity to host all the observed quasars. The nine luminous quasars at redshift  $5.7 < z < 6.5$  discovered by the SDSS (which all have black holes with mass  $M_{\text{BH}} = 1\text{--}4 \times 10^9 M_{\odot}$  via the Eddington argument) give a space density of  $(6.4 \pm 2.4) \times 10^{-10}$  Mpc $^{-3}$  (Fan et al. 2004).<sup>5</sup> The halo mass function at  $z = 6.3$  was determined from the mass function fitted to the numerical simulations of Sheth & Tormen (1999). The quasar space density corresponds to the space density of all halos with  $M_{\text{DM}} > 1.5 \times 10^{13} M_{\odot}$ . This limit is cosmology dependent and is obviously strongly dependent on the high-mass tail of the Sheth & Tormen mass function, which is only relatively sparsely sampled in the simulations used to determine this fit. However, in support of this functional form, Barkana & Loeb (2004) show that the tail provides a good approximation to the numerical mass function at extremely high redshifts, provided that the lack of large-scale modes in the simulations is taken into account.

An estimate of the host halo masses can be found by using the estimated black hole masses and further assuming that there is a

<sup>5</sup> We neglect the likely existence of quasars just as powerful as those in the SDSS that have their UV luminosities substantially decreased by dust. The space density of obscured quasars at lower redshifts is comparable to that of unobscured quasars (Zheng et al. 2004). However, the ratio of obscured to unobscured quasars at  $z = 6$  is so uncertain that we do not attempt to make any correction to the quasar space density.

correlation between black hole and halo masses. Such a correlation has been shown to exist at low redshifts (Ferrarese 2002) via a combination of the well-known stellar bulge–black hole mass correlation and a correlation between halo circular velocity and bulge velocity dispersion. The correlation determined by Ferrarese (2002), with a correction applied by Bromley et al. (2004), is

$$\frac{M_{\text{BH}}}{10^8 M_{\odot}} \sim 0.015 \left( \frac{M_{\text{DM}}}{10^{12} M_{\odot}} \right)^{1.82}. \quad (1)$$

The universality of this correlation is untested, and in particular whether it evolves with redshift is highly uncertain. We refer to this nonevolving correlation between  $M_{\text{BH}}$  and  $M_{\text{DM}}$  as case A.

Wyithe & Loeb (2003) have noted that in feedback-regulated black hole growth models (e.g., Silk & Rees 1998; Fabian 1999), the important parameter for the strength of the dark matter halo potential is the circular velocity, not the mass. The relationship between circular velocity and mass is redshift dependent due to the universal expansion:  $v_c \propto M_{\text{DM}}^{1/3} (1+z)^{1/2}$  (e.g., Barkana & Loeb 2001). The feedback-regulated model of Wyithe & Loeb<sup>6</sup> leads to a redshift-dependent correlation between  $M_{\text{BH}}$  and  $M_{\text{DM}}$  of

$$\frac{M_{\text{BH}}}{10^8 M_{\odot}} \sim f \left( \frac{M_{\text{DM}}}{10^{12} M_{\odot}} \right)^{5/3} (1+z)^{5/2}. \quad (2)$$

Since the dormant black holes observed in the local universe typically formed at redshifts  $1 < z < 2$  (e.g., Yu & Tremaine 2002), we fix the normalizing factor  $f$  so that the correlation roughly matches that of Bromley et al. (2004) at  $z = 1.5$ . This condition is met by  $f = 0.0018$ . We refer to this evolving correlation between  $M_{\text{BH}}$  and  $M_{\text{DM}}$  as case B.

Since the two possible scenarios are normalized to each other at  $z = 1.5$ , at higher redshifts the host halo for a black hole of a given mass is less massive for case B than case A. Specifically, for a quasar at  $z = 6.3$  with  $M_{\text{BH}} = 2 \times 10^9 M_{\odot}$ , case A gives  $M_{\text{DM}} = 5.2 \times 10^{13} M_{\odot}$  and case B gives  $M_{\text{DM}} = 1.3 \times 10^{13} M_{\odot}$ . A simple comparison of the case A estimate with the space-density limit shows that there are insufficient halos with masses of  $M_{\text{DM}} = 5 \times 10^{13} M_{\odot}$  at these high redshifts to host the number of observed quasars. The simple conclusion to draw is that the correlation between black hole mass and halo mass does not remain the same at  $z > 6$  as it is locally. A similar conclusion was reached by Bromley et al. (2004) by considering the total black hole mass density built up by quasars. Wyithe & Loeb (2005) showed that the evolution in the Two Degree Field (2dF) quasar correlation function over the (admittedly narrow) range  $1 < z < 2$  was more consistent with the evolving  $M_{\text{BH}}-M_{\text{DM}}$  correlation than with the redshift-independent one. In what follows we use both case A and B correlations, while remembering that prior evidence supports case B over case A.

An important ingredient in the application of such correlations that is often overlooked is the effect of intrinsic scatter in the relation. We now incorporate the scatter in these correlations to estimate the expected host halo masses. We show that including the scatter makes a significant difference due to the steepness of the halo mass function for these rare halos. This is

<sup>6</sup> We omit the parameter  $[\xi(z)]^{5/6}$  from the equation given in Wyithe & Loeb (2003), since it is close to unity and is negligible compared with the uncertainties involved.

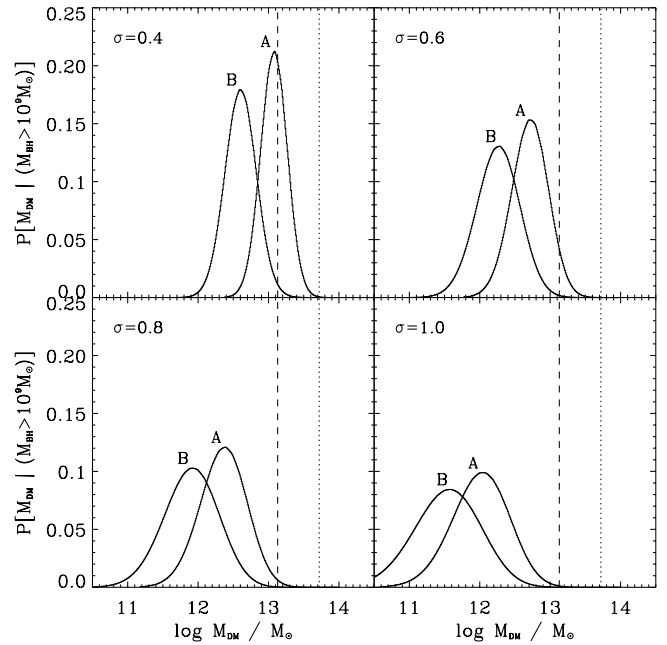


FIG. 5.—Probability distribution for the mass of the dark matter halo hosting a black hole with mass  $> 10^9 M_{\odot}$  at  $z = 6.3$ . These curves were generated assuming correlations between  $M_{\text{BH}}$  and  $M_{\text{DM}}$  of the forms A and B (see text), with lognormal intrinsic dispersion  $\sigma$ . The vertical dotted and dashed lines show the case A and case B  $M_{\text{DM}}$  expected for  $M_{\text{BH}} = 2 \times 10^9 M_{\odot}$  without considering the combined effects of scatter and the steepness of the halo mass function. These plots clearly show that the expected halo masses are considerably lower than those obtained by simply using the  $M_{\text{BH}}-M_{\text{DM}}$  correlation without scatter. [See the electronic edition of the Journal for a color version of this figure.]

because lower mass halos are much more abundant, so low-mass halos that are outliers in the  $M_{\text{BH}}-M_{\text{DM}}$  correlation could be more abundant than high-mass halos on the correlation.

We begin with the dark matter halo mass function fit of Sheth & Tormen (1999). This is evaluated at a redshift of  $z = 6.3$ . Above a mass of  $\sim 10^{12} M_{\odot}$ , the mass function exponentially declines. The black hole mass within each halo is given by the case A or case B correlations. We now add scatter to these black hole masses. The intrinsic scatter in the correlation between black hole mass and stellar velocity dispersion at low redshift is in the range 0.25–0.30 dex (Tremaine et al. 2002). The conversion from stellar velocity dispersion to halo mass is likely to add considerably more scatter, so we consider 0.4 dex to be the minimum amount of scatter in this correlation at low redshift. This scatter may increase substantially at higher redshifts, particularly for galaxies that are in the process of growing their black holes or accreting matter from the surrounding IGM. To bracket the uncertainty in the scatter, we consider four different cases with 0.4, 0.6, 0.8, and 1.0 dex scatter in the correlation. Although the shape of the scatter is unknown even locally, we adopt a lognormal distribution as the simplest shape.

By identifying the most luminous  $z \sim 6$  quasars across a large fraction of the sky, the SDSS has selected the most massive, active black holes at this epoch (under the assumption that luminous quasars at such early times are accreting at the Eddington limit). Therefore, we take a black hole mass cut of  $M_{\text{BH}} > 10^9 M_{\odot}$  and then calculate the probability distribution of dark matter halos that host such massive black holes given the correlations for cases A and B and the various amounts of scatter in the correlations. The results are shown in Figure 5.

Including scatter has considerably decreased the expected masses of the halos hosting these quasars. Even for the case with minimum scatter, there is a shift of  $\sim 0.5$  in  $\log M_{\text{DM}}$ . For the maximum scatter case considered, the shift in  $\log M_{\text{DM}}$  is  $\sim 1.5$ .

Walter et al. (2004) use resolved CO emission to measure a dynamical mass for the inner 2.5 kpc of SDSS J1148+5251 of  $\sim 5 \times 10^{10} M_{\odot}$ . They argued this to be at least a factor of 10 lower than expected by naive extrapolation of the low-redshift correlation between black hole mass and stellar velocity dispersion. We have shown here that using the case B redshift-dependent correlation and/or including the effects of a reasonable amount of scatter ( $\sigma \gtrsim 0.6$ ) lead to an expected halo mass at least an order of magnitude lower than using the naive correlation of case A. This provides a simple explanation for the observations of Walter et al. and those presented in this paper without the need for the  $M_{\text{BH}}-M_{\text{DM}}$  correlation to break down at high redshift. A consequence of this is that the SDSS quasars may not be identifying the most overdense regions of the high- $z$  universe, as is commonly assumed.

## 7. SUMMARY

We have presented deep imaging in the  $i'$  and  $z'$  filters of the fields of three of the most distant known quasars. For two of the three quasars, there are foreground galaxies at projected distances of a few arcseconds. However, the faintness of these galaxies suggests that they have relatively low masses, which, combined with the large impact parameters, provide only a weak gravitational lensing magnification that would not significantly alter the derived quasar luminosities.

A search for star-forming galaxies at the redshifts of the quasars was carried out. No enhancement in Lyman break galaxies above that in random fields is found. The UV continuum star formation limit reached is  $30 M_{\odot} \text{ yr}^{-1}$ , comparable with known  $z \approx 6.5$  galaxies. The lack of companion galaxies could indicate that these quasars reside in lower mass dark matter halos than previously believed. We consider the effect of scatter in correlations between black hole mass and halo mass and find that this scatter means that we expect the most massive black holes to be found in a range of halo masses, typically much lower than those found by use of a simple correlation between the two quantities.

To obtain a more accurate estimate of any overdensity of star-forming companions will require much deeper data. While few-orbit ACS observations are able to find a few possible companions (Stiavelli et al. 2005), a proper census requires something of similar depth to the Hubble Ultra Deep Field (reaching  $0.1L_{*}$  in the  $z = 6$  galaxy luminosity function, with a limiting magnitude of  $z' = 29$ ; Bunker et al. 2004), and such observations will therefore require a large increase in sensitivity, such as will be obtained from the *James Webb Space Telescope*.

Thanks to the Gemini North queue observers for executing the observations presented here. We thank Stuart Wytthe and Meghan Gray for interesting discussions. Thanks to the anonymous referee for some useful suggestions that improved the paper.

## REFERENCES

- Adelberger, K. L. 2005, *ApJ*, 621, 574  
 Barkana, R., & Loeb, A. 2001, *Phys. Rep.*, 349, 125  
 ———. 2004, *ApJ*, 609, 474  
 Bernardi, M., et al. 2003, *AJ*, 125, 1849  
 Bertin, E., & Arnouts, S. 1996, *A&AS*, 117, 393  
 Bertoldi, F., Carilli, C. L., Cox, P., Fan, X., Strauss, M. A., Beelen, A., Omont, A., & Zylka, R. 2003a, *A&A*, 406, L55  
 Bertoldi, F., et al. 2003b, *A&A*, 409, L47  
 Blain, A. W., Chapman, S. C., Smail, I., & Ivison, R. J. 2004, *ApJ*, 611, 725  
 Bolzonella, M., Miralles, J.-M., & Pelló, R. 2000, *A&A*, 363, 476  
 Bouwens, R. J., et al. 2004, *ApJ*, 606, L25  
 Bromley, J. M., Somerville, R. S., & Fabian, A. C. 2004, *MNRAS*, 350, 456  
 Bruzual, G., & Charlot, S. 2003, *MNRAS*, 344, 1000  
 Bunker, A. J., Stanway, E. R., Ellis, R. S., & McMahon, R. G. 2004, *MNRAS*, 355, 374  
 Capak, P., et al. 2004, *AJ*, 127, 180  
 Comerford, J. M., Haiman, Z., & Schaye, J. 2002, *ApJ*, 580, 63  
 Couchman, H. M. P., & Rees, M. J. 1986, *MNRAS*, 221, 53  
 Dickinson, M., et al. 2004, *ApJ*, 600, L99  
 Dunlop, J. S., McLure, R. J., Kukula, M. J., Baum, S. A., O'Dea, C. P., & Hughes, D. H. 2003, *MNRAS*, 340, 1095  
 Fabian, A. C. 1999, *MNRAS*, 308, L39  
 Fan, X., et al. 2001, *AJ*, 122, 2833  
 ———. 2003, *AJ*, 125, 1649  
 ———. 2004, *AJ*, 128, 515  
 Ferrarese, L. 2002, *ApJ*, 578, 90  
 Ferrarese, L., & Merritt, D. 2000, *ApJ*, 539, L9  
 Gebhardt, K., et al. 2000, *ApJ*, 539, L13  
 Giavalisco, M., et al. 2004, *ApJ*, 600, L93  
 Hu, E. M., Cowie, L. L., McMahon, R. G., Capak, P., Iwamuro, F., Kneib, J.-P., Maihara, T., & Motohara, K. 2002, *ApJ*, 568, L75  
 Hutchings, J. B., Frenette, D., Hanisch, R., Mo, J., Dumont, P. J., Redding, D. C., & Neff, S. G. 2002, *AJ*, 123, 2936  
 Kaiser, N. 1984, *ApJ*, 284, L9  
 Kashikawa, N., et al. 2004, *PASJ*, 56, 1011  
 Keeton, C. R., Kuhlen, M., & Haiman, Z. 2005, *ApJ*, 621, 559  
 Kodaira, K., et al. 2003, *PASJ*, 55, L17  
 Kukula, M. J., Dunlop, J. S., McLure, R. J., Miller, L., Percival, W. J., Baum, S. A., & O'Dea, C. P. 2001, *MNRAS*, 326, 1533  
 López-Cruz, O., Barkhouse, W. A., & Yee, H. K. C. 2004, *ApJ*, 614, 679  
 Madau, P., Pozzetti, L., & Dickinson, M. 1998, *ApJ*, 498, 106  
 Magorrian, J., et al. 1998, *AJ*, 115, 2285  
 Nagao, T., et al. 2004, *ApJ*, 613, L9  
 Pandey, B., & Bharadwaj, S. 2005, *MNRAS*, 357, 1068  
 Priddey, R. S., Isaak, K. G., McMahon, R. G., Robson, E. I., & Pearson, C. P. 2003, *MNRAS*, 344, L74  
 Richards, G. T., et al. 2004, *AJ*, 127, 1305  
 Ridgway, S. E., Heckman, T. M., Calzetti, D., & Lehnert, M. 2001, *ApJ*, 550, 122  
 Sheth, R. K., & Tormen, G. 1999, *MNRAS*, 308, 119  
 Shioya, Y., et al. 2002, *PASJ*, 54, 975  
 Silk, J., & Rees, M. J. 1998, *A&A*, 331, L1  
 Songaila, A., & Cowie, L. L. 2002, *AJ*, 123, 2183  
 Stiavelli, M., et al. 2005, *ApJ*, 622, L1  
 Tremaine, S., et al. 2002, *ApJ*, 574, 740  
 Walter, F., Carilli, C., Bertoldi, F., Menten, K., Cox, P., Lo, K. Y., Fan, X., & Strauss, M. 2004, *ApJ*, 615, L17  
 Walter, F., et al. 2003, *Nature*, 424, 406  
 Willott, C. J., McLure, R. J., & Jarvis, M. J. 2003a, *ApJ*, 587, L15  
 Willott, C. J., Rawlings, S., Jarvis, M. J., & Blundell, K. M. 2003b, *MNRAS*, 339, 173  
 Wytthe, J. S. B., & Loeb, A. 2002a, *Nature*, 417, 923  
 ———. 2002b, *ApJ*, 577, 57  
 ———. 2003, *ApJ*, 595, 614  
 ———. 2005, *ApJ*, 621, 95  
 Yamada, S. F., et al. 2003, *PASJ*, 55, 733  
 Yu, Q., & Tremaine, S. 2002, *MNRAS*, 335, 965  
 Zheng, W., et al. 2004, *ApJS*, 155, 73